Tectonophysics xxx (2013) xxx–xxx

Contents lists available at SciVerse ScienceDirect

Tectonophysics

journal homepage: www.elsevier.com/locate/tecto

Seismic structure in the southeastern China using teleseismic receiver functions

Qiusheng Li [a,b,*], Rui Gao [a,b], Francis T. Wu [c], Ye Guan [a,b], Zhuo Ye [a,b], Qimin Liu [d], Hao Kuo-Chen [e], Rizheng He [a,b], Wenhui Li [a,b], Xuzhang Shen [f]

[a] Institute of Geology, CAGS [1], Beijing, 100037, China
[b] Key Laboratory of Earthprobe and Geodynamics, CAGS, Beijing, 100037, China
[c] Department of Geological Sciences, State University of New York, Binghamton, NY 13902-6000, USA
[d] Institute of Tibetan Plateau Research, CAS, Beijing, 100085, China
[e] Institute of Geophysics, National Central University, Chungli, 32001, Taiwan
[f] Lanzhou Institute of Seismology, China Earthquake Administration, Lanzhou, 730000, China

ARTICLE INFO

Article history:
Received 4 September 2012
Received in revised form 31 May 2013
Accepted 30 June 2013
Available online xxxx

Keywords:
Receiver functions
SE China
Moho
LAB
Mantle transition zone

ABSTRACT

The southeastern margin of China is an ideal area to study the modern plate interactions. The previous models, however, are poorly constrained with respect to the geometry due to the sparse coverage. Here we present new observations from a temporary array with 20 stations in southeastern China.

We isolated converted seismic phases in the P and S wave coda to generate receiver function from the structure of the crust and upper mantle. By using H–K stacking and common conversion point stacking, the geometry of discontinuities above was imaged along the southeastern Chinese coastline. The CCP section shows Moho dips gently northeastward with a mean depth of 30 km. The 410 and 660 km discontinuities are at the depth close to IASP91 model. This means that we have not seen any significant anomaly from Moho and mantle transition zone that corresponded with the geodynamics of plate subducting, instead, we found that the crust was ruptured by Min River fault to depth of the Moho.

We provide a 2D map of Moho topography by combining our crustal thickness to that from permanent stations, active seismic and OBS offshore profiles. The map is consistent with previous studies and shows a crust that thins coastward and southwestward in the rate of ~1.5 km per 100 km. We image the lithosphere–asthenosphere boundary at a depth of 60 to 70 km by using S-wave to combine with the P-wave.

Our crustal structure suggests that Min River fault certainly plays an important role in adjusting regional stress field induced by plate interactions in the study area. Our lithospheric thickness is more consistent with a very strongly attenuated continental lithosphere. Given the close proximity to the coast this might suggest that the lithospheric mantle transitions to oceanic before the crust does. Alternatively, we may infer that the continental lithosphere has been thermally eroded in this region.

1. Introduction

Southeast (SE) China is located at the southeastern margin of the Eurasian plate, which is also characterized by widespread Jurassic to Cretaceous igneous rocks (Li et al., 2007; Zhou and Li, 2000) and strong plate interaction among the Eurasia, the Philippine Sea (Pacific), and the India plates in tectonics.

The origin of the Late Mesozoic igneous rocks and the interaction among the Pacific or Philippine Sea, the Eurasian, and the Indian plates has been studied over the past decade or more years (e.g. Chen et al., 2004, 2005; Chi et al., 2003; Kao et al., 1998, 2000; Wu et al., 1997, 2009; Zhang et al., 2005, 2008, 2012; Zhao et al., 2013). Several tectonic models, such as mantle plume, mantle-wedge, flat-slab subduction and an alternative model, have been proposed to illustrate the lithospheric deformation induced by plate interactions or distribution feature of Mesozoic to Cenozoic igneous rocks in the study region and adjacent area based on geophysical or geochemical data (e.g. Li et al., 2009; Zhao, 2004; Zhao et al., 2013). Result from seismic receiver function and tomography revealed the crustal and mantle structural heterogeneities down to 800 km in depth that provided clear evidence of the Eurasian plate is being subducted beneath southwestern Taiwan and the Philippine Sea plate is descending steeply beneath northeastern Taiwan (e.g. Bijwaard et al., 1998; Cheng, 2009; H. Huang et al., 2010; Huang and Zhao, 2006; Kuo-Chen et al., 2012; Li et al., 2009; T.K. Wang et al., 2006; Wu et al., 2007; Z.C. Huang et al., 2010; Z. Wang et al., 2006; Zhao, 2004).

* Corresponding author at: Institute of Geology, CAGS, Beijing, 100037, China. Tel.: +86 1068999834.
E-mail address: liqiusheng@cags.ac.cn (Q. Li).
[1] *CAGS* is the abbreviation of "Chinese Academy of Geological Sciences".

0040-1951/$ – see front matter © 2013 Published by Elsevier B.V.
http://dx.doi.org/10.1016/j.tecto.2013.06.033

The crustal thickness, Poisson's ratio, and the mantle transition zone (MTZ) thickness as well as 3D P-wave velocity structure of the upper mantle in this study region have been presented using the data from portable and permanent seismic stations (Ai et al., 2007; H. Huang et al., 2010; Huang and Zhao, 2006; Z.C. Huang et al., 2010). However, due to the sparse coverage of permanent stations and deficiency of lateral constraint, geodynamics of this region remain not well understood. For the purpose of imaging the high-resolution structure of the crust and upper mantle of SE China, we deployed 20 broadband stations along the southeastern margin of the China Mainland between August 2008 and May 2011. The teleseismic P-wave receiver functions (Farra and Vinnik, 2000; Langston, 1977; Vinnik, 1977) are used to detect seismic waves converted from the crust–mantle boundary (Moho discontinuity) and discontinuities at 410 km and 660 km that confined the mantle transition zone (MTZ) (Bostock, 1996). In addition, S-wave receiver functions are also used to identify the lithosphere–asthenosphere boundary (LAB). Our results show that the crust thickness decreases coastward and reach a mean depth of 30 km, while the LAB is located at depths ~60 to ~70 km. The results provide a new constraint for the dynamics model of plate interactions of SE China and imply that the transition from oceanic to continental lithosphere occurs more quickly than the transition from oceanic to continental crust.

2. Data acquisition and methodology

2.1. Data acquisition

One of the objectives of the Sinoprobe Project is to image the three-dimensional structure in the southeastern China continent (Dong et al., 2013 – in this issue). In this study, we deployed a linear array that was composed of a total of 20 temporary broadband stations at an interval of 30–50 km along the southeastern coast of Mainland China (Fig. 1 and Table 1). Each station was allocated with RT130 recorder (REFTEK) with the CMG-3ESP or CMG-3T sensors (Guralp). All of the stations operated continuously from August 2008 to June 2011 with a sample rate of 50 samples per second.

The teleseismic events in the epicentral distance range between 30° and 95° with magnitude (Ms) greater than 5.5 were selected according to the NEIC catalogue. Fig. 2 shows that most of the events are located between back azimuth 270–45° (Eurasia continent, Japanese sea and northwestern Pacific) and 110–225° (the southwestern Pacific) around the study region (center at 120° E, 25.50° N). Among those events, only those distances between 60° and 85° and Ms greater than 5.6 are used for S-wave receiver function analysis.

2.2. Receiver function methodology

2.2.1. Receiver function construction

The three-component seismograms were rotated into the vertical, radial and transverse components before simultaneously deconvolving and migrating to depth according to the one-dimensional velocity model IASP91 (Kennett and Engdahl, 1991). Our results are potentially affected by strong lateral variations of ratios between the P-wave and S-wave velocity (Vp/Vs) that do not match IASP91. In this study, the local crustal velocity model from H. Huang et al. (2010) and Z.C. Huang et al. (2010) and the active seismic profile (J.F. Zhu et al., 2005; Liao et al., 1988) are used to improve the IASP91 reference model.

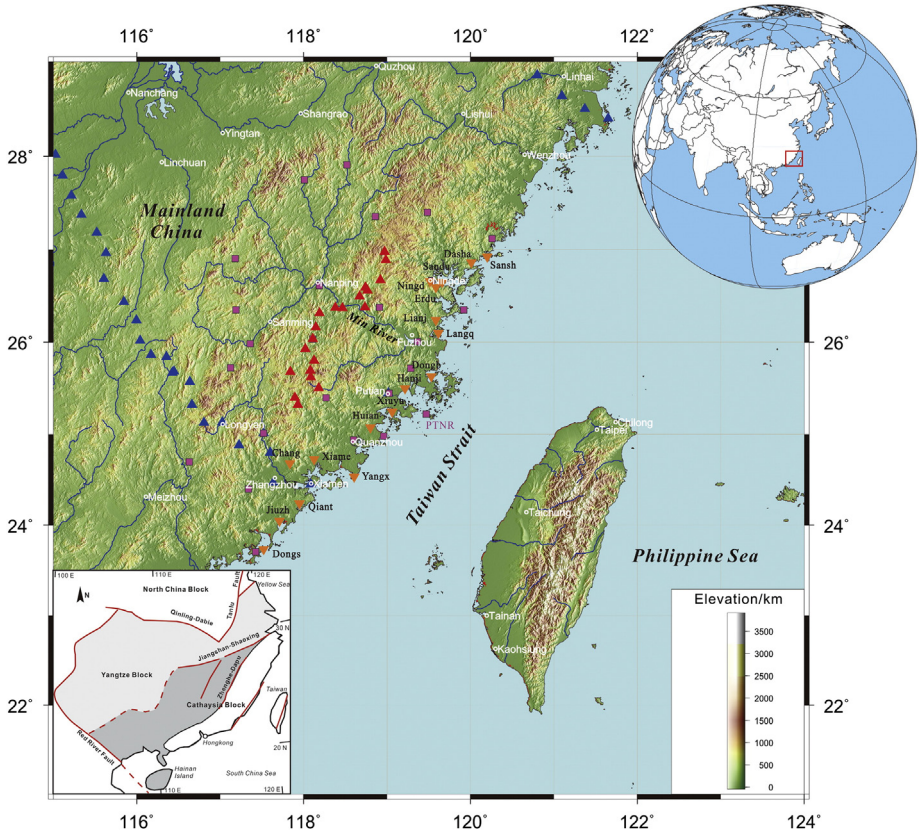

Fig. 1. Deployment map of the 20 temporary broadband stations (orange diamond) in southeastern China (2008.08–2011.06). Codes with four or more capital letters near orange diamond or red triangle (a new deployment since July, 2011) are station names. The blue triangles show two associate temporary broadband arrays (H. Huang et al., 2010; Z.C. Huang et al., 2010; the upper right unpublished); the rivers are shown in blue carves and faults in red lines (the lower left insert), respectively. The city or town is marked in white circles with capital. The insert diagram at the upper right corner shows the position of the study area in global map and the insert at the low left corner show the tectonic setting of the study area (modified from Xu et al., 2007). The pink squares show the permanent stations of NCDSN in study area. (For interpretation of the references to color in this figure legend, the reader is referred to the web version of this article.)

Please cite this article as: Li, Q., et al., Seismic structure in the southeastern China using teleseismic receiver functions, Tectonophysics (2013), http://dx.doi.org/10.1016/j.tecto.2013.06.033

Table 1
Vp/Vs ratio and crustal thickness of the stations along coastline profile, SE China.

Order	Station	Latitude	Longitude	Vp/Vs	H	Quantity
1	Sansh	26.923	120.198	1.79	31.0	59
2	Dasha	26.860	120.012	1.82	31.5	51
3	Ningd	26.661	119.514	1.77	31.0	16
4	Sandu	26.651	119.660	1.77	31.5	33
5	Erdu	26.594	119.584	1.80	31.0	93
6	Lianj	26.242	119.583	1.75	33.0	12
7	Langq	26.099	119.616	1.78	31.5	40
8	Dongb	25.628	119.528	1.80	29.5	51
9	Hanj	25.500	119.214	1.80	29.0	20
10	Xiuyu	25.243	119.06	1.76	29.5	18
11	Hui'an	25.070	118.801	1.72	29.5	29
12	Yangx	24.533	118.606	1.78	28.5	48 + 30
13	Xiame	24.727	118.124	1.83	29.5	14
14	Changt	24.678	117.836	1.76	31.0	26
15	Qiant	24.238	117.951	1.76	29.0	35 + 44
16	Jiuzh	24.046	117.708	1.77	29.0	33 + 9
17	Dongs	23.734	117.521	1.79	27.5	20

In total 856 teleseismic three-component waveforms were used for calculating receiver functions by using the method of Zhu (2004). A Gaussian parameter (alpha = 2.5), which excludes frequencies over about 1.2 Hz (Ammon, 1991) was adopted in the deconvolution and the resultant receiver functions were windowed from 10 s before and 80 s after the first P-wave phase, respectively. We manually inspected each event-station pair to ensure the impulsive sharp P phase and the clear P-to-S phase converted from the Moho.

As shown in Fig. 3, the PmS arrival time is fairly constant with moderately strong amplitude (the raw traces with a signal-to-noise ratio >5, approaching 10). It can be clearly identified at ~4.0 s and its PpPs multiples are at 12 to 14 s. From the raw receiver function of station Jiuzh (top diagram of Fig. 3. This station is located at the Southwest end of the coastline profile). There is an abnormal phase ahead of Pms phase in the RF section of Sansh (bottom diagram of Fig. 3. This station is located near the Northeast end of the coast profile). Fig. 4a shows all individual raw P-receiver functions plotted within a time window of 0–30 s after the direct P arrival for all 20 stations in trace spacing. All the traces are moveout-corrected to a constant ray parameter of 0.0573 s/km (corresponding to a slowness of 6.4 s/° or an epicentral distance of 67°) using the IASP91 reference model. The PmS and its multiple phases PpPs are obvious, and a local arrival delay of both Pms and PpPs can be seen between station Dongb and Liangj.

3. Data analysis and results

3.1. Data analysis

The iterative deconvolution was originally used to estimate source time functions for large-earthquakes (Kikuchi and Kanamori, 1982), then it was developed by Ligorria and Ammon (1999) and Zhu (2004) to calculate receiver functions.

Time Domain Receiver Function methods have been widely used to image the deep structure of the Earth since they were introduced to seismology about three decades ago (Langston, 1977; Owens et al., 1984; Vinnik, 1977). Two methods utilizing arrival times of Ps and its multiple phases, H–k (Chevrot and van der Hilst, 2000; Zhu and Kanamori, 2000) and common conversion-point (CCP) stacking techniques (Dueker and Sheehan, 1997; Yuan et al., 1997) were used in this study.

The H–k method has the advantage of objectively determining an optimal crustal thickness. However, it requires that we assume a

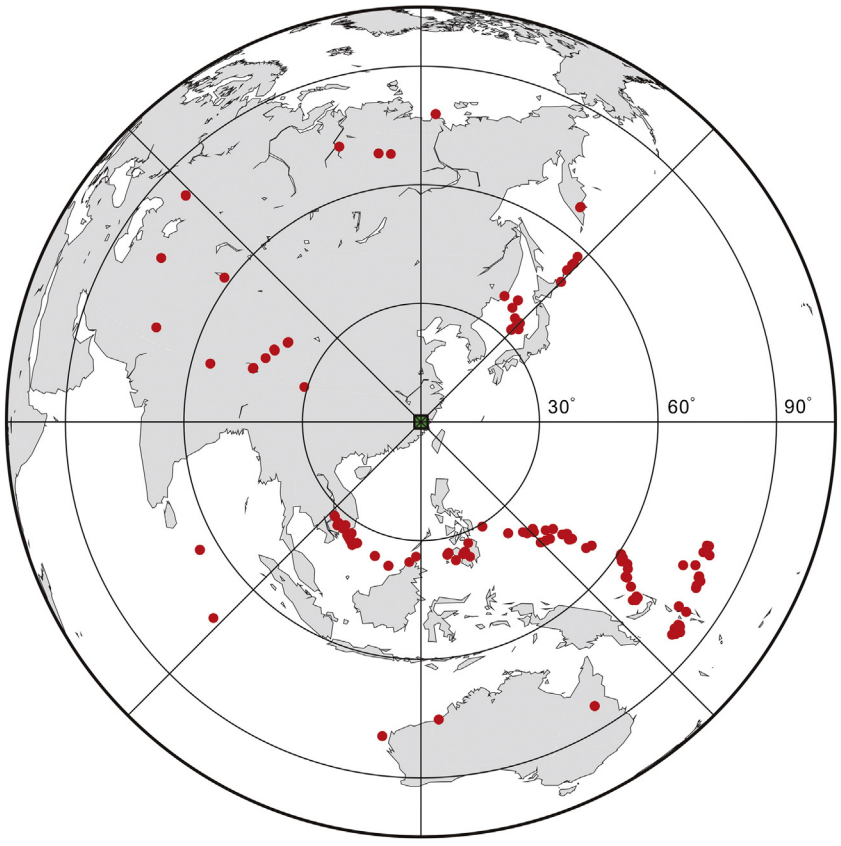

Fig. 2. Distribution of teleseismic events used in this study (epicentral distance 30–95°, Ms > 5.5). Only the event distances 60–85°, Ms > 5.6, for S-wave receiver function.

Please cite this article as: Li, Q., et al., Seismic structure in the southeastern China using teleseismic receiver functions, Tectonophysics (2013), http://dx.doi.org/10.1016/j.tecto.2013.06.033

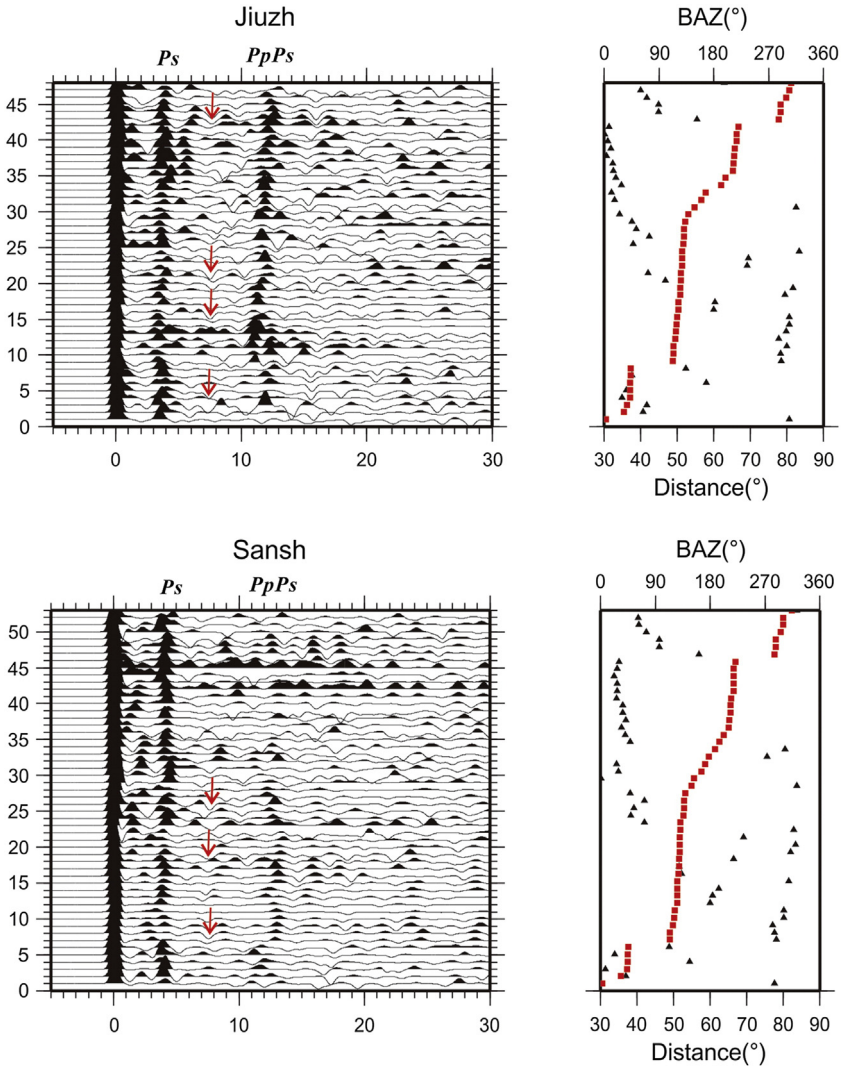

Fig. 3. Raw receiver functions of individual stations, sorted by back azimuth. The top panels show the receiver functions from Jiuzh station. The below panels show the receiver functions from Sansh station. The phases are labeled at the top side of the left diagram and the series number of receiver function at the left side. The red square dot and black triangle in the right diagram of each station denote the distribution of the effective events. Red squares show back azimuth and black triangles show epicenter distances; the PmS phase are obvious around 4.0 s and a negative phase can be seen following it at 7.0 to 7.5 s (as the red arrow indicated). (For interpretation of the references to color in this figure legend, the reader is referred to the web version of this article.)

P-wave velocity and a uniform Vp/Vs and crustal thickness for each station (Zandt and Ammon, 1995).

CCP stacking technique (Kosarev et al., 1999; Zhu, 2000, 2002) was performed to constrain the lateral variation of crustal and upper mantle discontinuities beneath the study region.

The P-receiver function method is one of the most reliable approaches to studying the Moho and upper mantle discontinuities, but can be limited to image the LAB because the P-to-S phases from LAB are often contaminated by crustal multiples. To avoid this problem, S-wave receiver function can be used. The other advantage of the S-wave receiver function is the amplitude of S-to-P phase may be higher than the corresponding P receiver function (Wittlinger and Farra, 2007) and the reverberations from shallow structures in the P-wave receiver functions are not present in the S-receiver functions.

The S-wave receiver function analysis needs higher quality waveforms than P-wave receiver function because of other phases near the S phase. In this study, only the teleseismic events $Ms > 5.6$ with epicentral distances in the range of 60°to 85°were chosen for generating S receiver functions to avoid late arriving teleseismic P wave multiples.

A three order low-pass filter (2 s) was applied to the origin waveforms. Zero time is the S-arrival time. The N–E–Z components were rotated to R–T–Z coordinate system according to the theoretical back azimuth. R and Z are then rotated into the P–SV system. The incident angle is changed from 0 to 60° with a 2-degree step. For each step, the S receiver function is constructed by deconvolving the SV component from the P component. The deconvolution is performed in time domain described by Kumar et al. (2006), and the time axis is reversed to compare with the P receiver function.

3.2. Main results

3.2.1. Crustal thickness and Vp/Vs ratio

The H–k stacking results at all stations are shown in Table 1. The crustal thickness and Vp/Vs ratios are well constrained for each station (Fig. 5a).

Along the coast, H varies in a range of 27.5 to 33.0 km with an average of 30.3 km, slightly dipping northeastward. The largest crustal thickness is beneath the station Lianj (33 km) and crustal thickness in the northeast systemically increases comparing to the 10 stations in the southwest. Nearly all the former is larger than 31 km, and the

Please cite this article as: Li, Q., et al., Seismic structure in the southeastern China using teleseismic receiver functions, Tectonophysics (2013), http://dx.doi.org/10.1016/j.tecto.2013.06.033

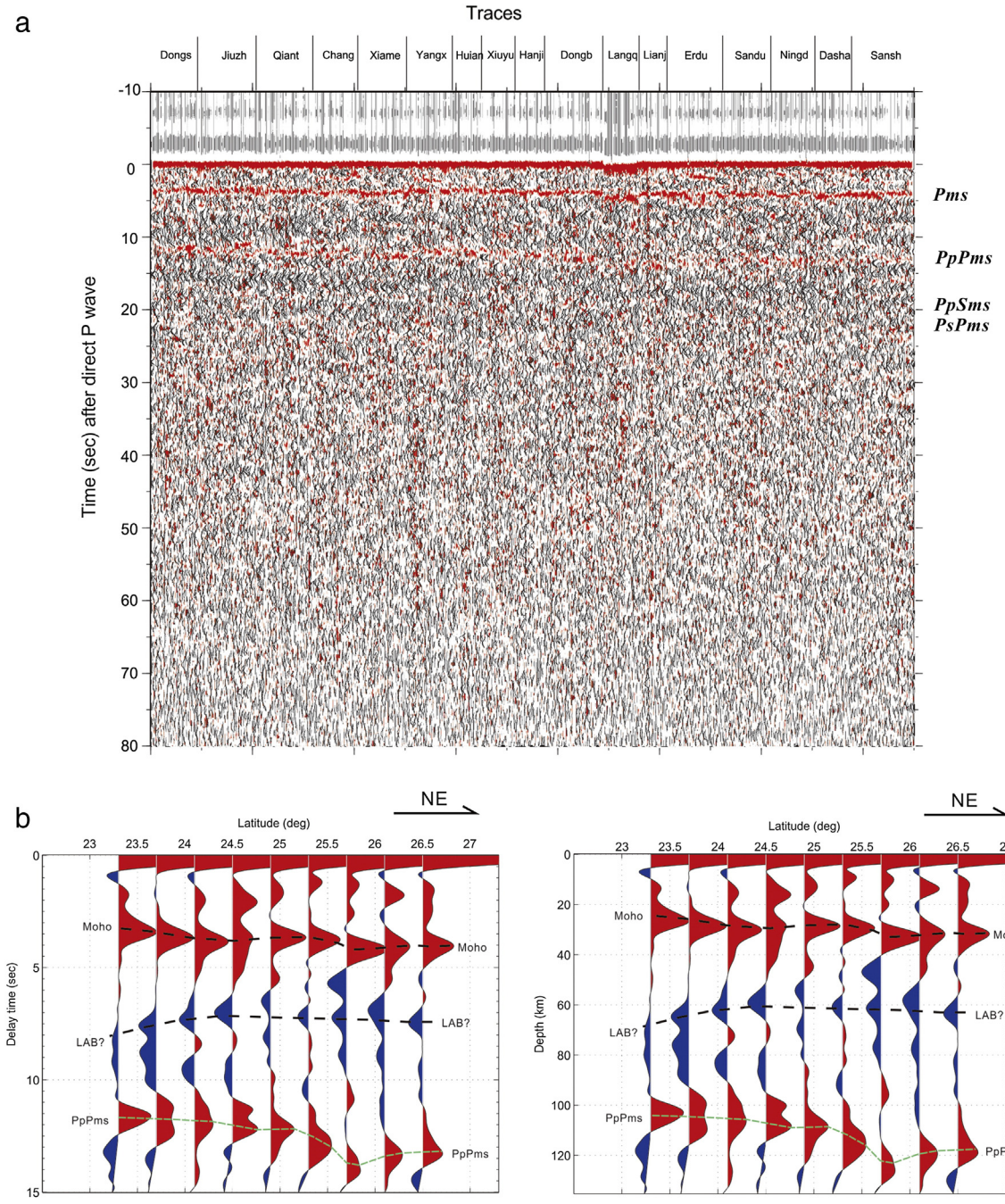

Fig. 4. The raw P-wave receiver functions and binning stacked view. (a) P-wave receiver functions of all stations along the coastline profile (approximately NE36.5°), sorted for each station by incident angle and ray paths. The phases are marked on the right side, respectively. (b) Binning stacked view of P-wave receiver function, sorted by latitude of the stacking bins along coast profile. The bin size is set at 200 km in width and about 65 km along the profile. Seismic events from the southeast (back azimuth: 90°–135°) were used for the stacking and the traces are moveout-corrected to a slowness 6.4 s/°. The left: the image in time domain; the right: the migrated image in depth domain. The phases such as Pms, PLABS and multiples of PmS have been marked in the diagrams by black, blue and green dashed line, respectively. (For interpretation of the references to color in this figure legend, the reader is referred to the web version of this article.)

largest (33 km) is at the station Lianj near the Min River (Fig. 1). The later is less than 30 km except Changt station. The crust is thinner at least 2 km between the stations Dongb and Langq to Lianj where the Min River Fault crosses (Fig. 1). It is important to note that these modest changes in crustal thickness could also reflect variations in bulk crustal velocity. Most of the Vp/Vs ratios are larger than 1.76 except at the station Hui'an. Vp/Vs ratios vary from 1.72 to 1.83 with a mean of 1.78 along the coastline.

A 2D contour map of the Moho depth has been made (Fig. 5b) by combining the results of H–k stacking from permanent station array (the original waveform for two years recorded by New China Digital Seismology Network (NCDSN)) and the results from Ocean Bottom Seismograph (OBS) profiles (Gao et al., 2004; Mcintosh et al., 2005; T.K. Wang et al., 2006; Yeh et al., 1998). It is consistent with previous studies (Ai et al., 2007; H. Huang et al., 2010; Li et al., 2010) and provides sufficient details to characterize the topography of the Moho discontinuity in our study region.

In Fig. 5b, the Moho dips slightly to the northeast and the crust thins along coastal belt than in hinterland. The thinnest crust in the study area appears at the Guangzhou Bay, the northern margin of

Please cite this article as: Li, Q., et al., Seismic structure in the southeastern China using teleseismic receiver functions, Tectonophysics (2013), http://dx.doi.org/10.1016/j.tecto.2013.06.033

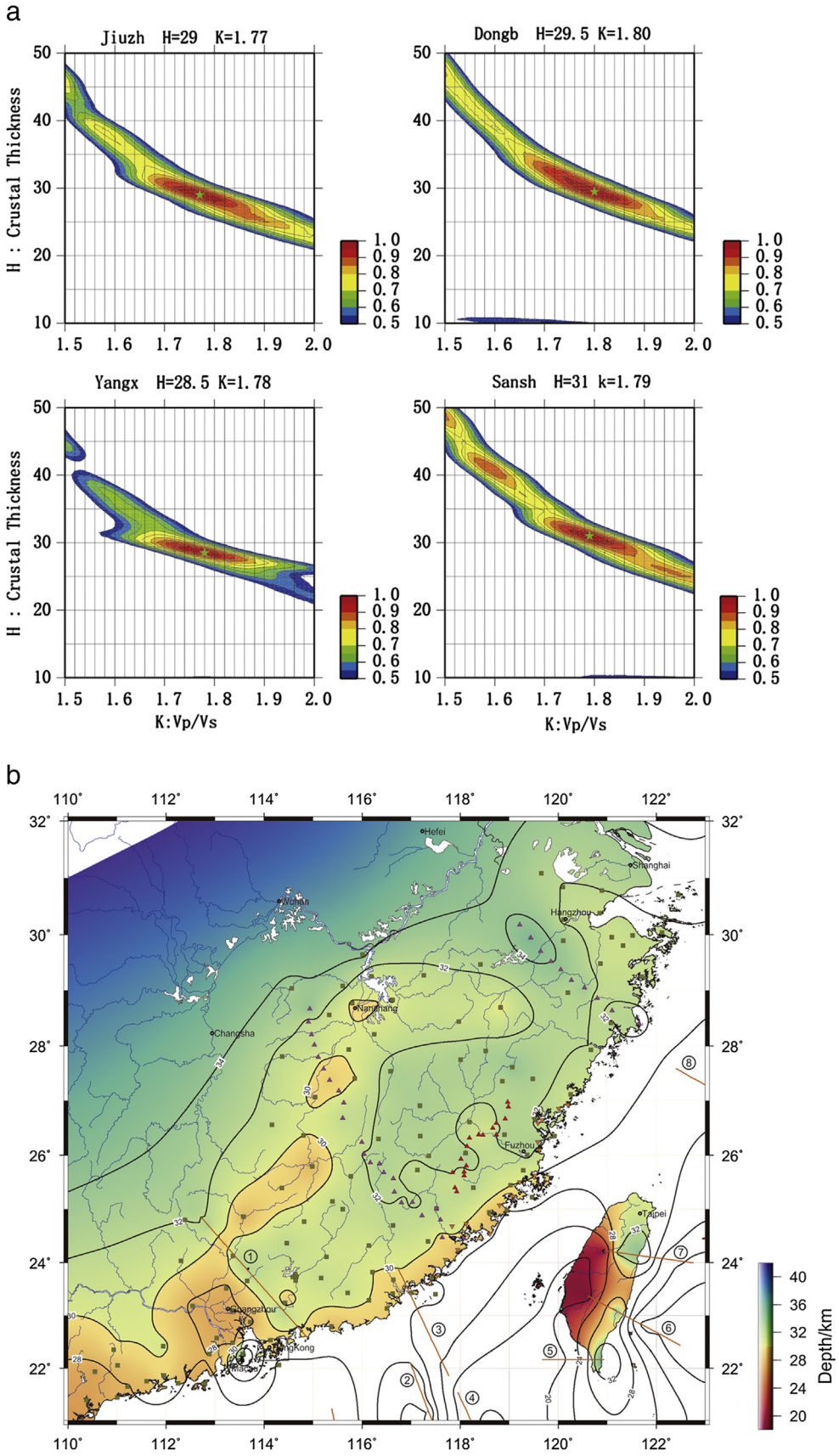

Fig. 5. Examples of the H–k stacking and 2D map of crustal thickness. (a) 4 examples of the H–k stacking. The colors show stacking values, the star symbols denote the best estimations of crustal thickness (H) and Vp/Vs ratios (K). The station name, H and K is labeled at the top side of each diagram. (b) 2D Moho depth map of the coast zone and adjacent area. The map is made from the data of passive observations and active seismic profiles. The squares show the permanent stations of NCDSN; the red and dark triangle show 4 temporary broadband profile (Fig. 1); the red line shows explosive wide-angle and OBS profile: ①—Zhang et al., 2012; ②—Nissen et al., 1995; ③, ④—Zhao et al., 2004; T.K. Wang et al., 2006; ⑤—Yeh et al., 1998; ⑥, ⑦—McIntosha et al., 2005; ⑧—Gao et al., 2004. (For interpretation of the references to color in this figure legend, the reader is referred to the web version of this article.)

Please cite this article as: Li, Q., et al., Seismic structure in the southeastern China using teleseismic receiver functions, Tectonophysics (2013), http://dx.doi.org/10.1016/j.tecto.2013.06.033

the South China Sea basin. The map also shows a region where the Moho is deeper than 30 km, which has been commonly accepted as the eastern part of Cathaysia Block is railed off by a bulge belt (depth less than 30 km) with a few isolated lump in north and northwest (Xu et al., 2007).

3.2.2. P-wave CCP stacking section

A CCP stacking algorithm (Kosarev et al., 1999; Zhu, 2000, 2002) was used to image the geometry of the crustal and upper mantle discontinuities beneath the southeastern margin of Mainland China. Our CCP stacking profile has an azimuth of approximately N36.5° E roughly parallel to the coast (Fig. 1). The CCP stacking image is sensitive to the velocity structure. To determine optimal 1D crustal structure model (Kennett and Engdahl, 1991; Wu and Zeng, 1998), both the previous results from receiver function (H. Huang et al., 2010; Li et al., 2009) and active source seismic profiles (J.F. Zhu et al., 2005; Liao et al., 1988) was used for improving the IASP 91 model. A bin size of 1 km along the profile and 1 km in depth was taken for CCP stacking and total 756 reliable receiver functions were used to construct the CCP image (Fig. 6a).

The CCP section provides a geometric constraint of crustal and upper mantle discontinuities along the coastline. Along the profile, the Moho is clearly identified as a strong positive conversion phase at 28 to 30 km depths. The Moho dips gently northeastward and sharply breaks right beneath the Minjiang fault zone between 26.2 and 26.3° (Figs. 6b and 1). It indicates the Min River fault ruptured the crust down to the Moho and thus may play an important role in adjusting regional stress field to a certain extent.

The 410-km and 660-km discontinuities are imaged at the mean depths of the global IASP91 (Kennett and Engdahl, 1991; Houser and Williams, 2010) and consistent with ambient level in Eurasia (Kustowski et al., 2008) along the profile in the map of piercing point (Fig. 6a and c). We were not able to image any significant anomalies from MTZ, e.g. apparent anti-correlated changes in topography corresponded with subducted slab or hot plume. A normal MTZ (thick 250 ± 5 km) implies that the mantle transition zone beneath the southeastern margin of China is not disturbed by sinking slabs or rising plumes.

3.2.3. Identification of LAB

Besides positive phases i.e. Moho, 410-km and 660-km discontinuities, we have observed signatures of the LAB using the P- and S-wave receiver functions (Figs. 4b and 6b). A negative polarity phase can be obviously seen between 60 and 70 km below the Moho in Fig. 6b (marked in black dash line). The negative signal is very clear; we are even able to observe negative polarity phases in the raw receiver functions (Fig. 3). It is visible and is not contaminated by late multiples of PmS. The raw receiver functions were repeated processing with different band-passed filter: 2 s–20 s, 3 s–20 s and 5 s–50 s, the negative signal is consistently observed at 7 s with very little temporal variation. If these signals were effects of prestack filtering then we would expect to see systematic variations in arrival times with different filters (alphas). Although it closely follows the PmS phase, the negative polarity signal after the Moho is difficult to infer as the side lobe of PmS phase because it also looks not exactly symmetrical not only the waveform but also the distance to the main lob.

Usually even after a band-pass filtering, the $P_{LAB}S$ phases are still difficult to be identified in the raw receiver functions. The CCP stack and/or migration are standard tools that are used to detect LAB reverberations. We stack the P-wave receiver functions in the range of 30

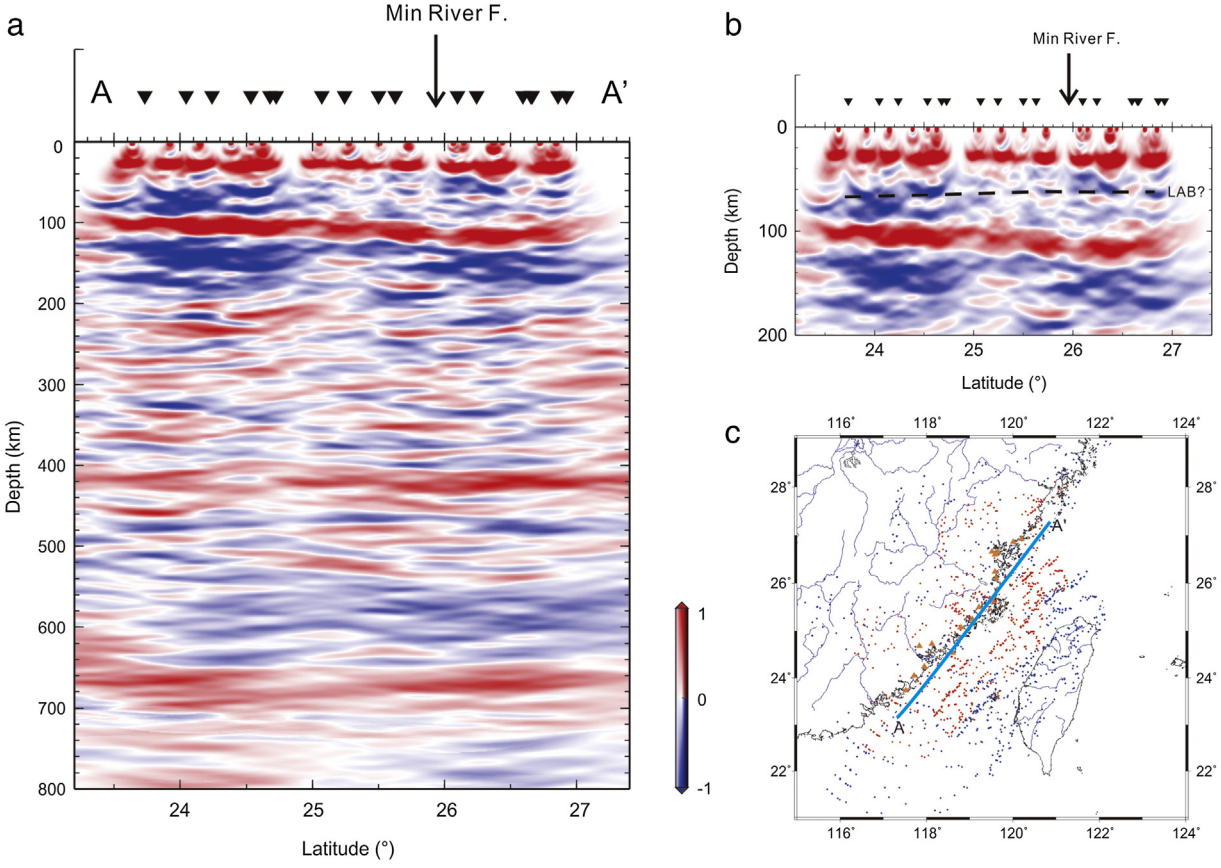

Fig. 6. (a) ~800 km depth section view of P-wave receiver function; (b) ~200 km depth section view of crustal and lithosphere. The red and blue colors showing the positive and negative stacking amplitude, respectively. (c) distribution map of piercing point of the 410 (red dot) and 660 (blue dot). (For interpretation of the references to color in this figure legend, the reader is referred to the web version of this article.)

Please cite this article as: Li, Q., et al., Seismic structure in the southeastern China using teleseismic receiver functions, Tectonophysics (2013), http://dx.doi.org/10.1016/j.tecto.2013.06.033

to 90° (epicentral distances) in a bin size of 200 km in width and about 65 km along the profile, as a result the negative polarity phase consistently arrives at 7.0 s (the left diagram, Fig. 4b), which corresponds to a depth of 60 to 70 km (the right diagram, Fig. 4b).

Along much of the profile the negative polarity phase follows the Moho phase closely. However, we observe a deviation in the relative arrival of the two phases between 23 and 25° (Fig. 4b) and that was revealed more obvious between negative polarity phase and PpPs (the multiples of PmS).

The relative arrival between negative polarity phase and PmS as well as its multiples was also checked by using the data of permanent stations of NCDSN near the coastal profile (an example shown as Fig. 7). The negative polarity phase is distinct and independent of PmS in the raw receiver functions (Fig. 7a) and stack section (Fig. 7b) of time domain or the migrated section of depth domain (Fig. 7c).

The negative polarity phase, being always allied to a structure with negative velocity gradients, could represent either P to S conversions at the base of lithospheric discontinuity or PpPs multiples from a crustal interface (Chen et al., 2006). Along the whole profile, there are few identifiable signals coherent with the crustal structure. In contrast, an obvious mantle phase can be continuously detected at 7.0–7.5 s with a nearly horizontal geometry. For further excluding the possibility of PpPs multiple phases from an inverse crustal structure, after band-pass filtering then multiple phase's move-out correction was applied to the raw receiver function. As shown in Fig. 7d, the geometry of the PpPs become sub horizontal but the candidate for $P_{LAB}S$ dips apparently toward the orientation of epicentral distance decreasing in the section. In summary, the negative polarity signal is difficult to infer as the side lobe of PmS phase and crustal multiples, although it follows the Moho closely and arrives too early to a normal continent LAB conversion.

S-wave receiver functions have been proved commonly, although not always, to be able to detect the signals from the LAB due to the absence of multiples (e.g. Kumar et al., 2006). In order to confirm the negative polarity amplitudes as upper mantle structure, we performed a deconvolution of S receiver function in time domain. We tested a large number of filters, similar to the approach we used with the P wave receiver functions. The raw S receiver functions are shown in Fig. 8a. The Sp conversion from the Moho (positive amplitudes) and the $S_{LAB}P$ (negative amplitudes) are visible in Fig. 8a (as labeled). The negative polarity phase of S-receiver functions arrives at approximately to that at the P-receiver functions in Fig. 4b and Fig. 6b, although they do not have identical piercing points. The similarity between P and S receiver functions also indicates that this is a real conversion from upper mantle structure instead of a side lobe or crustal multiples.

For suppressing noise and enhancing spatial consistency of direct S-to-P conversion phase from the LAB, we continuously performed a move-out corrected stack of raw S receiver function in time domain with a constant ray parameter of 0.0573 s/km (corresponding to a

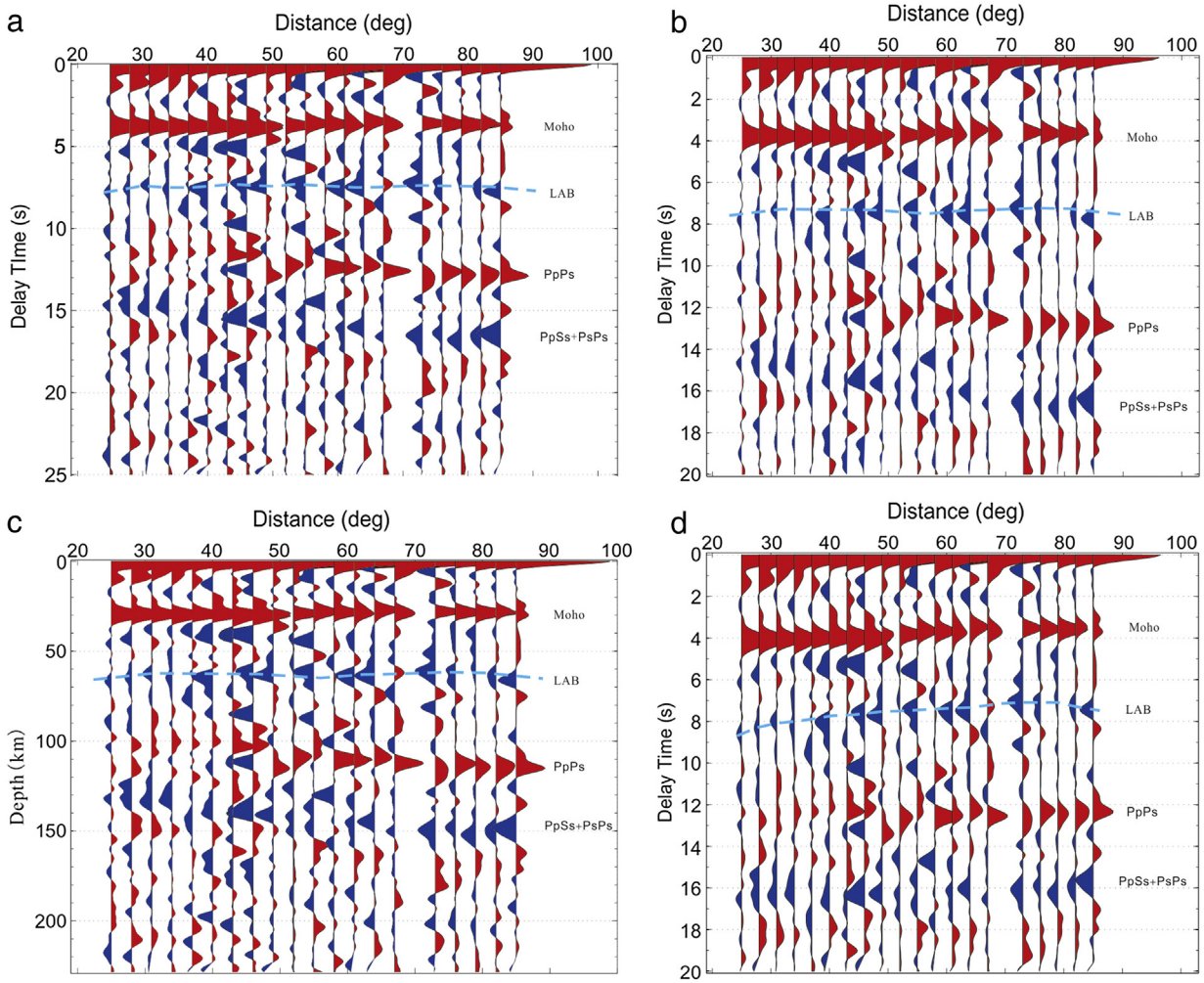

Fig. 7. Binned receiver functions of permanent station PTNR (see square labeled with PTNR in Fig. 1) sorted by epicentral distances. Receiver functions are stacked in a bin size of 3° from 25° to 95°. (a) Raw receiver functions after a band-pass filtering; (b) moveout-corrected section by Ps phase; (c) migrated section using IASP91 as reference model; (d) moveout-corrected section by PpPs multiple phase.

Please cite this article as: Li, Q., et al., Seismic structure in the southeastern China using teleseismic receiver functions, Tectonophysics (2013), http://dx.doi.org/10.1016/j.tecto.2013.06.033

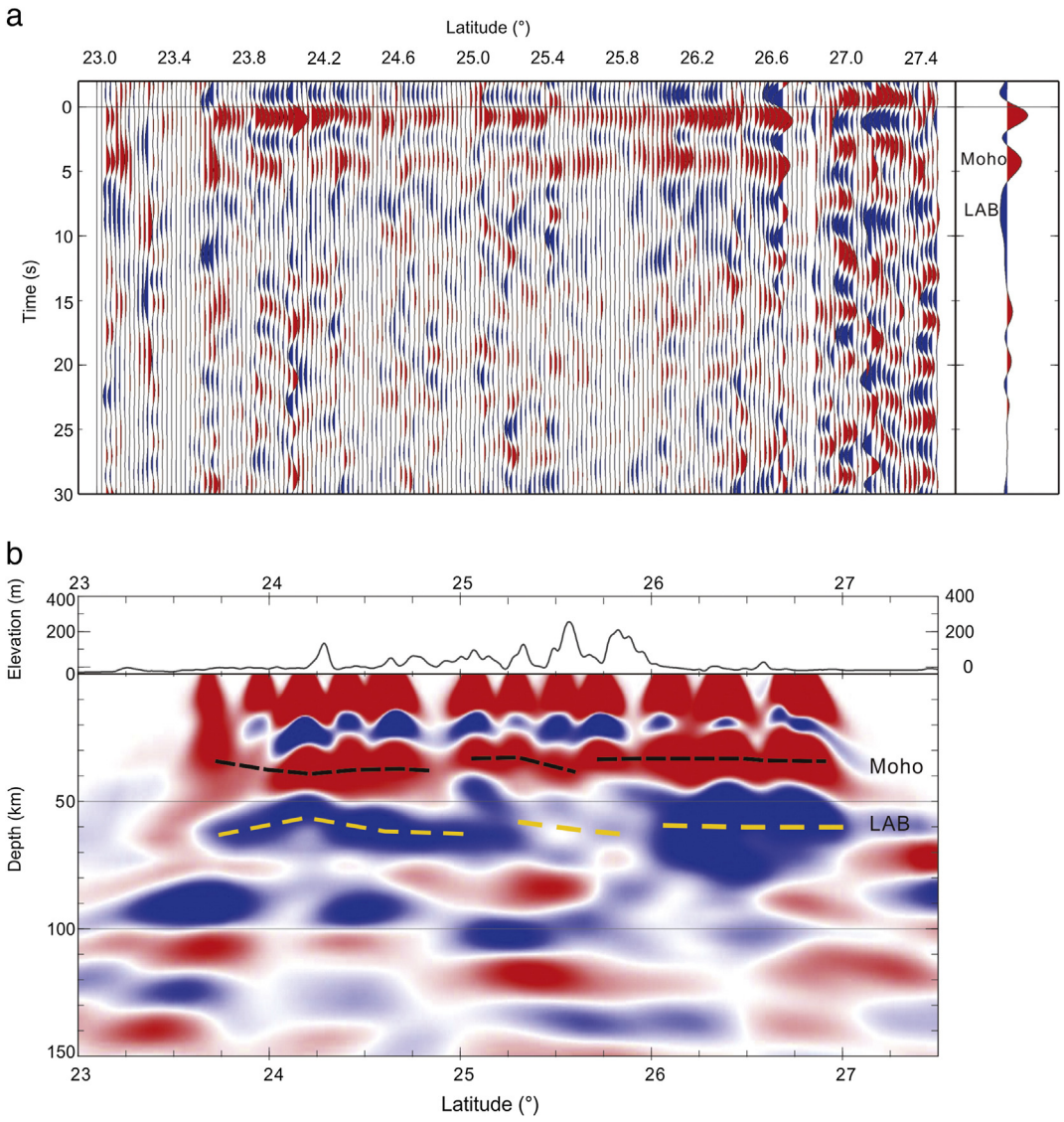

Fig. 8. The raw S-wave receiver functions (a) and migrated section (b). (a) Raw S-wave receiver functions of all station in time domain; (b) migrated section base on IASP 91 global model. The Moho and LAB are marked in black and orange yellow dash line, respectively. The red color represents the positive (indicate velocity decease upward) phase and the blue represents the negative (indicate the velocity increase upward) phase. (For interpretation of the references to color in this figure legend, the reader is referred to the web version of this article.)

slowness of 6.4 s/° or an epicentral distance of 67°), and then migrated it into depth domain referring the IASP91 model. As show as Fig. 8b, The negative polarity phase in the migrated section of S receiver function was imaged at depth range of 60 to 70 km beneath the coast belt. The preliminary results from the inland profile, which lies nearly parallel to the coast profile off 150 km to the north (marked in red triangle in Fig. 1), show similar crustal and upper mantle structure besides slightly thicker lithosphere (Huang et al., 2009; Ye et al., 2013).

In short words, we have assumed the negative polarity phase both in P wave and S wave receiver functions is the conversion from the base of the lithosphere, i.e. LAB phase. This result reveals that the coast belt (perhaps include South China Sea) overlies thin lithosphere. This conclusion agrees with the results of surface wave tomography studies (Huang et al., 2009; J.S. Zhu et al., 2005), in which the lithosphere thins to coast in large gradient along southeastern and eastern margin of Eurasia continent.

4. Discussion and conclusions

Comparing to previous regional results (e.g. Ai et al., 2007; H. Huang et al., 2010; Li et al., 2009; Yuan and Zheng, 2009), our results using the new dataset provide more detailed structural properties in SE China and adjacent region. The coastline profile provides important constraints on the crustal thickness. The CCP section reveals the Min River fault extending through a crust scale, and perhaps cuts the section into the southwestern and northeastern segment based upon thickness and structural complexity. Such results might hint that a three-dimensional image of the crustal structure is required in this region.

In order to construct a 2D map of the crustal thickness (Fig. 5b), we used relative variations in crustal thickness derived from our receiver function data combined with assumptions of the absolute crustal thickness in the hinterland and foreland. We used the following formula:

$$(H1-H2)/D*100\%, \quad (1)$$

where H1, H2 represent the crustal thicknesses of hinterland or at the northern margin of South China and coastline of SE China, respectively. D represents the distance from the coastline to hinterland. By taking 35 km (Nissen et al., 1995; Huang et al., 2008; Wang et al.,

unpublished[2]) as H1, 29 km as H2 (H. Huang et al., 2010) and 400 km as D. The crustal thins coastward at an approximate rate of about 1.5 km per 100 km, which is approximately same as that derived from an adjacent wide angle seismic profile (Zhang et al., 2012).

We have observed the Moho discontinuity at an average depth of 30 km in the study area; however, we also found a ~2 km increase in Wuyishan area. The thick crustal domain is half-circled by a thinner crustal zone with a few isolated bulges from the north and northwest. We infer it should be relevant to Wuyishan as the core part of the 'Cathaysia old continent' in geological history (Grabau, 1924).

Global surface-wave studies (Kustowski et al., 2008; Lebedev and van der Hilst, 2008; Nettles and Dziewonski, 2008) have imaged rigid lithospheres increasing in thickness from oceans to continents. However, the depth resolution of most surface- and body-wave tomography studies is limited to 40 km or larger. Regional observations of sharp velocity decreasing with depth at the LAB have been obtained worldwide using P-to-S, S-to-P conversion and multi-S waves by Rychert and Shearer (2009). Lateral variations in depth likely occur at finer scales, as seen in large-scale regional results (Kustowski et al., 2008; Li and Burke, 2006; Simons et al., 1999).

In this study, we identified LAB phase by combining P-wave receiver function with S-wave receiver function and then imaged it at depth of 60 to 70 km along the coastline. This thickness is scarce for a typical stable continental lithosphere but thin lithosphere has been reported previously (Huang et al., 2009; J.S. Zhu et al., 2005) from surface wave tomography, although there is not obvious presentation of LAB in recent larger scale body-wave tomography work by Z.C. Huang et al. (2010).

Our crustal thickness values would suggest the crust is continental, given it is probably too thick to be oceanic; however our lithospheric thickness values are more consistent with oceanic lithosphere or very strongly attenuated continental lithosphere. Given the close proximity to the coast, this might suggest that the lithospheric mantle transitions to oceanic before the crust does. Alternatively, we may infer that the continental lithosphere has been thermally eroded in this region.

Several conceptual models have been proposed to explain the geodynamic processes affecting eastern China during Mesozoic to Cenozoic time: the mantle plume, mantle-wedge, flat-slab subduction and an alternative model related to thick craton lithosphere root (e.g. Li et al., 2007, 2009; Zhao, 2004; Zhao et al., 2013). Among these conceptual models, the mantle-wedge model suggests that horizontal mantle flow would strongly influence the area overlying the subducting slab front, similar to that of the western margin of the North America continent (Burdick et al., 2012; Schmandt et al., 2012). This case would lead to extension and evident "basin and range province" type topography in the Cathaysia Block. This model seems closely consistent with the observation of lithosphere entirely thinning beneath the southeastern margin of China mainland. However, there are no significant anomalies (e.g. apparent anti-correlated changes in lithospheric topography corresponded with subducted slab or hot plume) to be found at MTZ beneath SE China and/or coastal belt previously (Ai et al., 2007) and in this study. Therefore, our observations do not support the model of typical mantle-wedge and/or plume-like hot mantle. Zhao et al. (2013) proposed an alternative scenario that emphasizes interactions between thick lithospheric roots of the Yangtze craton and the ocean-plate subduction-induced mantle flow. Zhao's Model can explain NE–SW to ENE–WSW trending fast directions (imprint of lithosphere extending in this orientation) with a deflect mantle flow but fails to account for NE–SW strike variation of crustal thickness in Cathaysia Block (Fig. 2). Finally, the flat-slab subduction model (Li et al., 2007) suggests large scale lithosphere slab down-going and regional hot mantle matter upwelling that would generate symmetrical anisotropic features. Therefore obvious fast or slow wave direction shouldn't have been detected in Cathaysia Block. This hypothesis is obviously inconsistent with the facts of SKS shear wave splitting measurements (Zhao et al., 2013).

Instead we would suggest that our observations show evidence of lithosphere thinning involved along the SE China coastline. We infer that the crustal deformational features are mainly induced by regional tectonic events of large scale extension during Mesozoic (~65 Ma), which have been widely accepted. The thickness and attitude of lithosphere are yet the reflection of a strong eroding process prior to initiation of the Philippine Sea plate subduction (Wan and Zhao, 2012). We tend to link the lithospheric thinning to the event occurred between 32 Ma and 17 Ma, which results in formation of the South China Sea basin and perhaps has a large influence on the study area. In any case, our observations provide new constraints for plate interactions and dynamics on the southeast margin of the SE China.

Acknowledgments

This research is supported by the Special Funds for Sciences and Technology Research of Public Welfare Trades (grant No. 201011042, i.e. Sinoprobe-02-03), the National Natural Science Foundation of China (Grant Nos. 40874045 and 41174081) the Land Resource Survey Project of China Geological Survey (grant No. 1212010611809) and US NSF project TAIGER at the data processing stage. We sincerely thank Mr. Shen Jiangsheng and his staffs for their help during the field work in Fujian provinces. The discussions with Prof. Wang Liangshu (Nanjing University, China), Prof. Shi Danian (Institute of Mineral and Resource, CAGS) and Dr. Li Yonghua (Institute of Geophysical, CEA) were very helpful. Special also to the anonymous reviewers who provided constructive review comments and English revising, which greatly improved the manuscript. Most of the figures were made by using Generic Mapping Tools (Wessel and Smith, 1995, 1998).

References

Ai, Y.S., Chen, Q.F., Zeng, F., Hong, X., Ye, W.Y., 2007. The crust and upper mantle structure beneath southeastern China. Earth and Planetary Science Letters 260, 549–563.

Ammon, C.J., 1991. The isolation of receiver function effects from teleseismic P waveforms. Bulletin of Seismological Society of America 81, 2504–2510.

Bijwaard, H., Spakman, W., Engdahl, R., 1998. Closing the gap between regional and global travel time tomography. Journal of Geophysical Research 103, 30055–30078.

Bostock, M.G., 1996. Ps conversions from the upper mantle transition zone beneath the Canadian landmass. Journal of Geophysical Research 101, 8393–8402.

Burdick, S., van der Hilst, R.D., Vernon, F.L., Martynov, V., Cox, T., Rakins, J., Karasu, G.H., Tylell, J., Astiz, L., Pavlis, G.L., 2012. Model update March 2011: upper mantle heterogeneity beneath North America from Traveltime Tomography with Global and USArray Transportable Array Data. Seismological Research Letters 83 (1), 23–28. http://dx.doi.org/10.1785/gssrl.83.1.23.

Chen, P.F., Huang, B.S., Liang, W.T., 2004. Evidence of a slab of subducted lithosphere beneath central Taiwan from seismic waveforms and travel times. Earth and Planetary Science Letters 229, 61–71.

Chen, X., Lin, S., Li, Z., Bao, T., Zhou, Z., 2005. Preliminary 1D model for crust velocity structure in Fujian—Taiwan region. Earthquake 25, 61–68 (In Chinese with English abstract).

Chen, L., Zheng, T., Xu, W., 2006. A thinned lithospheric image of the Tanlu Fault Zone, eastern China: constructed from wave equation based receiver function migration. Journal of Geophysical Research 111, B09312. http://dx.doi.org/10.1029/2005JB003974.

Cheng, W., 2009. Tomographic imaging of the convergent zone in Eastern Taiwan—a subducting forearc sliver revealed? Tectonophysics 466, 170–183.

Chevrot, S., van der Hilst, R.D., 2000. The Poisson ratio of the Australian crust: geological and geophysical implications. Earth and Planetary Science Letters 183, 121–132.

Chi, W.C., Reed, D.L., Moore, G., Nguyen, T., Liu, C.S., Lundberg, N., 2003. Tectonic wedging along the rear of the offshore Taiwan accretionary prism. Tectonophysics 374, 199–217.

Dong, S.W., Li, T.D., Lü, Q.T., Gao, R., Yang, J.S., Chen, X.H., Wei, W.B., Zhou, Q., (2013 – in this issue). Progress in deep lithospheric exploration of the continental China: a

[2] Wang Liangshu et al., The crustal and upper mantle structure in Lower Yangze and its adjacent region. Post. The International Symposium on Deep Exploration into the Lithosphere, 2011, Beijing China.

Please cite this article as: Li, Q., et al., Seismic structure in the southeastern China using teleseismic receiver functions, Tectonophysics (2013), http://dx.doi.org/10.1016/j.tecto.2013.06.033

review of the SinoProbe. Tectonophysics. http://dx.doi.org/10.1016/j.tecto.2013.05.038.
Dueker, K.G., Sheehan, A.F., 1997. Mantle discontinuity structure from midpoint stacks of converted P to S waves across the Yellowstone hotspot track. Journal of Geophysical Research 102 (4), 8313–8327.
Farra, V., Vinnik, L., 2000. Upper mantle stratification by P and S receiver function. Geophysical Journal International 141, 699–712.
Gao, D.Z., Zhao, J.H., Bo, Y.L., Tang, J., Wang, S.J., 2004. A profile study of gravidities—magnetic and seismic comprehensive survey in the East China Sea. Chinese Journal of Geophysics 47 (5), 853–861 (in Chinese with English abstract).
Grabau, A.W., 1924. Stratigraphy of China, Part I, Paleozoic and Older. Geological Survey of Agriculture and Commence, Peking 528.
Houser, C., Williams, Q., 2010. Reconciling Pacific 410 and 660 km discontinuity topography, transition zone shear velocity patterns, and mantle phase transitions. Earth and Planetary Science Letters 296, 255–266.
Huang, J.L., Zhao, D.P., 2006. High-resolution mantle tomography of China and surrounding regions. Journal of Geophysical Research 111, B09305. http://dx.doi.org/10.1029/2005JB004066.
Huang, J.P., Chong, J.J., Ni, S.D., 2008. Inversing the crustal thickness under the stations of China via H-Kappa method. Journal of University of Science and Technology of China 38 (1), 33–40 (In Chinese with English abstract).
Huang, Z.X., Xu, Y., Hao, T.Y., Peng, Y.J., Zheng, Y.J., 2009. Surface wave tomography of lithospheric structure in the seas of East China. Chinese Journal of Geophysics 52 (2), 379–389.
Huang, H., MI, N.*., Xu, M.J., WANG, L.S., LI, H., YU, D.Y., 2010. S-wave velocity structures of the crust and uppermost mantle, and Poisson ratios in Fujian Province. Geological Journal of China Universities 16 (4), 465–474.
Huang, Z.C., Wang, L.S., Zhao, D.P., Xu, M.J., Mi, N., Yu, D.Y., Li, H., Li, C., 2010. Upper mantle structure and dynamics beneath Southeast China. Physics of the Earth and Planetary Interiors 182, 161–169.
Kao, H., Shen, S., Ma, K., 1998. Transition from oblique subduction to collision: earthquakes in the southernmost Ryukyu arc—Taiwan region. Journal of Geophysical Research 103, 7211–7229.
Kao, H., Huang, G., Liu, C., 2000. Transition from oblique subduction to collision in the northern Luzon arc—Taiwan region: constraints from bathymetry and seismic observations. Journal of Geophysical Research 105, 3059–3080.
Kennett, B.L.N., Engdahl, E.R., 1991. Travel times for global earthquake location and phase identification. Geophysical Journal International 105, 429–465.
Kikuchi, M., Kanamori, H., 1982. Inversion of complex body waves. Bulletin of the Seismological Society of America 72, 491–506.
Kosarev, G., Kind, R., Sobolev, S.V., Yuan, X., Hanka, W., Oreshin, S., 1999. Seismic evidence for a detached Indian lithospheric mantle beneath Tibet. Science 283 (5406), 1306–1309.
Kumar, P., Yuan, X.H., Kind, R., Ni, J., 2006. Imaging the colliding Indian and Asian lithospheric plates beneath Tibet. Journal of Geophysical Research 111, B06308. http://dx.doi.org/10.1029/2005JB003930.
Kuo-Chen, H., Wu, F.T., Roecker, S.W., 2012. Three-dimensional P velocity structures of the lithosphere beneath Taiwan from the analysis of TAIGER and related seismic datasets. Journal of Geophysical Research. http://dx.doi.org/10.1029/2011JB009108.
Kustowski, B., Ekstrom, G., Dziewonski, A.M., 2008. The shear-wave velocity structure in the upper mantle beneath Eurasia. Geophysical Journal International 174, 978–992.
Langston, C.A., 1977. The effect of planar dipping structure on source and receiver responses for constant ray parameter. Bulletin of the Seismological Society of America 67, 1029–1050.
Lebedev, S., van der Hilst, R.D., 2008. Global upper-mantle tomography with the automated multimode inversion of surface and S-wave forms. Geophysical Journal International 173, 505–518.
Li, A.B., Burke, K., 2006. Upper mantle structure of southern Africa from Rayleigh wave tomography. Journal of Geophysical Research 111, B10303. http://dx.doi.org/10.1029/2006JB004321.
Li, X.H., Li, Z.-X., Li, W.X., Liu, Y., Yuan, C., Wei, G.J., Qi, C.S., 2007. U–Pb zircon, geochemical and Sr–Nd–Hf isotopic constraints on age and origin of Jurassic I- and A-type granites from central Guangdong, SE China: a major igneous event in response to foundering of a subducted flat-slab? Lithos 96, 186–204.
Li, Z., Xu, Y., Hao, T., Xu, Y., 2009. Vp and Vp/Vs structures in the crust and upper mantle of the Taiwan region, China. Science in China Series D 52, 975–983.
Li, Q.S., Gao, R., He, C.S., Guan, Y., 2010. The differ respond of China continental to the collision between Eurasian and Philippine plate. Eos, Transactions of the American Geophysical Union 91 (47) (Fall Meeting abstract).
Liao, Q.L., Wang, Z.M., Wang, P., Yu, Z.K., 1988. Explosion seismic study of the rustal structure in Fuzhou–Quanzhou–Shantou region. Acta Geophysica Sinica 31 (3), 270–280.
Ligorria, J.P., Ammon, C.J., 1999. Iterative deconvolution and receiver-function estimation. Bulletin of the Seismological Society of America 89 (5), 1395–1400.
McIntosha, K., Nakamuraa, Yosio T., Wang, T.-K., Shih, R.-C., Chen, A., Liu, C.-S., 2005. Crustal-scale seismic profiles across Taiwan and the western Philippine Sea. Tectonophysics 401, 23–54.
Nettles, M., Dziewon'ski, A.M., 2008. Radially anisotropic shear velocity structure of the upper mantle globally and beneath North America. Journal of Geophysical Research 113, B02303. http://dx.doi.org/10.1029/2006JB004819.
Nissen, S., Hayes, D., Buhl, P., Diebold, J., Yao, B., Zeng, W., Chen, Y., 1995. Deep penetration seismic sounding across the north margin of South China Sea. Journal of Geophysical Research 100 (B11), 22407–22433.
Owens, T.J., Zanda, G., Taylor, S.R., 1984. Seismic evidence for an ancient rift beneath the Cumberland Plateau, Tennessee: a detailed analysis of broadband teleseismic P waveforms. Journal of Geophysical Research 89 (B9), 7783–7795.
Rychert, C.A., Shearer, P.M., 2009. A global view of the lithosphere–asthenosphere boundary. Science 324, 495–498. http://dx.doi.org/10.1126/science.1169754.
Schmandt, B., Dueker, K., Humphreys, E., Hansen, S., 2012. Hot mantle upwelling across the 660 beneath Yellowstone. Earth and Planetary Science Letters 331–332, 224–236.
Simons, F.J., Zielhuis, A.D., van der Hilst, R., 1999. The deep structure of the Australian continent from surface wave tomography. Lithos 48, 17–43.
Vinnik, L.P., 1977. Detection of waves converted from P to SV in the mantle. Physics of the Earth and Planetary Interiors 15, 39–45.
Wan, T.F., Zhao, Q.L., 2012. The genesis of tectono-magmatism in eastern China. Science China Earth Sciences 55. http://dx.doi.org/10.1007/s11430-011-4361-4.
Wang, T.K., Chen, M.K., Lee, C.S., Xia, K., 2006. Seismic imaging of the transitional crust across the northeastern margin of the South China Sea. Tectonophysics 412, 237–254.
Wang, Z., Zhao, D.P., Wang, J., Kao, H., 2006. Tomographic evidence for the Eurasian lithosphere subducting beneath south Taiwan. Geophysical Research Letters 33, L18306. http://dx.doi.org/10.1029/2006GL027166.
Wessel, P., Smith, W.H.F., 1995. New version of the Generic Mapping Tools (GMT) version 3.0 released. Eos, Transactions of the American Geophysical Union 76, 329.
Wessel, P., Smith, W., 1998. New improved version of the Generic Mapping Tools released. Eos, Transactions of the American Geophysical Union 79, 579.
Wittlinger, G., Farra, V., 2007. Converted waves reveal a thick and layered tectosphere beneath the Kalahari super-carton. Earth and Planetary Science Letters 254, 404–415.
Wu, Q.J., Zeng, R.S., 1998. The crustal structure of Qinghai–Xizang plateau inferred from broadband teleseismic waveform. Chinese Journal of Geophysics 41, 669–679 (in Chinese with English abstract).
Wu, F.T., Rau, R.J., Salzberg, D.H., 1997. Taiwan orogeny: thin skinned or lithospheric collision? Tectonophysics 274, 191–220.
Wu, Y., Chang, C., Zhao, L., Shyu, B., Chen, Y., Sieh, K., Avouac, J., 2007. Seismic tomography of Taiwan: improved constraints from a dense network of strong motion stations. Journal of Geophysical Research 112, B08312.
Wu, F.T., Liang, W.T., Lee, J.C., Benz, H., Villasenor, A., 2009. A model for the termination of the Ryukyu subduction zone against Taiwan: a junction of collision, subduction/separation, and subduction boundaries. Journal of Geophysical Research 114, B07404. http://dx.doi.org/10.1029/2008JB005950.
Xu, Xisheng, Suzanne, Y., Reilly, O., Griffinb, W.L., Wang, X.L., Pearson, N.J., Hea, H.Y., 2007. The crust of Cathaysia: age, assembly and reworking of two terranes. Precambrian Research 158, 51–58.
Ye, Z., Li, Q.S., Gao, R., Guan, Y., He, R.Z., Wang, H.Y., Lu, Z.W., Xiong, X.S., Li, W.H., 2013. Seismic receiver functions revealing crust and upper mantle structure beneath the continental margin of southeastern China. Chinese Journal of Geophysics (accepted for publication).
Yeh, Y.H., Shih, R.C., Lin, C.H., Liu, C.C., Yen, H.Y., Huang, B.S., Liu, C.S., Chen, P.Z., Huang, C.S., Wu, C.J., 1998. Onshore/offshore wide-angle deep seismic profiling in Taiwan. TAO 9 (3), 301–316.
Yuan, L.W., Zheng, S.H., 2009. Moho depths beneath broad-band stations in Fujian area inversed by teleseismic receiver function. South China Journal of Seismology 29 (3), 85–97 (In Chinese with English abstract).
Yuan, X., Ni, J., Kind, R., Mechie, J., Sandvol, E., 1997. Lithospheric and upper mantle structure of southern Tibet form a seismological passive source experiment. Journal of Geophysical Research 102 (B12), 27491–27500.
Zandt, G., Ammon, C.J., 1995. Continental crust composition constrained by measurements of crustal Poisson's ratio. Nature 374, 152–154.
Zhang, Z.J., Badal, J., Li, Y., Chen, Y., Yang, L.Q., Teng, J.W., 2005. Crust–upper mantle seismic velocity structure across Southeastern China. Tectonophysics 395, 137–157.
Zhang, Z.J., Zhang, X., Badal, J., 2008. Composition of the crust beneath Southeastern China derived from an integrated geophysical dataset. Journal of Geophysical Research 113. http://dx.doi.org/10.1029/2006JB004503.
Zhang, Z.J., Xu, T., Zhao, B., 2012. Systematic variations in seismic velocity and reflection in the crust of Cathaysia: new constraints on intraplate orogeny in the South China continent. Gondwana Research. http://dx.doi.org/10.1016/j.gr.2012.05.018.
Zhao, D., 2004. Global tomographic images of mantle plumes and subducting slabs: insight into deep Earth dynamics. Physics of the Earth and Planetary Interiors 146, 3–34.
Zhao, M.H., Qiu, X.L., Ye, C.M., Xia, K.Y., Huang, C.L., Xie, J.B., Wang, P., 2004. Analysis on deep crustal structure along the onshore–offshore seismic profile across the Binhai (Littoral) fault zone in northeastern South China Sea. Chinese Journal of Geophysics 47 (5), 845–852 (In Chinese with English abstract).
Zhao, L., Zheng, T.Y., Lu, G., 2013. Distinct upper mantle deformation of cratons in response to subduction: constraints from SKS wave splitting measurements in eastern China from SKS wave splitting measurements in eastern China. Gondwana Research. http://dx.doi.org/10.1016/j.gr.2012.04.007.
Zhou, X.M., Li, W.X., 2000. Origin of Late Mesozoic igneous rocks in Southeastern China: implications for lithosphere subduction and underplating of mafic magmas. Tectonophysics 326, 269–287.
Zhu, L.P., 2000. Crustal structure across the San Andreas Fault, Southern California from teleseismic converted waves. Earth and Planetary Science Letters 179, 183–190.
Zhu, L.P., 2002. Deformation in the lower crust and downward extent of the San Andreas Fault as revealed by teleseismic waveforms. Earth, Planets and Space 54, 1005–1010.
Zhu, L.P., 2004. Lateral variation of the Tibetan lithospheric structure inferred from teleseismic waveforms. In: Chen, Y.T., et al. (Ed.), Advancements in Seismology and Physics of the Earth Interior in China. Seismological Press, Beijing, pp. 295–310 (In Chinese).

Please cite this article as: Li, Q., et al., Seismic structure in the southeastern China using teleseismic receiver functions, Tectonophysics (2013), http://dx.doi.org/10.1016/j.tecto.2013.06.033

Zhu, L.P., Kanamori, H., 2000. Moho depth variation in southern California from teleseismic receiver functions. Journal of Geophysical Research 105, 2969–2980.

Zhu, J.F., XU, X.W., Zhang, X.K., Huang, Z.L., Chen, X.X., Fang, S.M., Liu, B.J., Zheng, R.Z., 2005. Joint exploration of crustal structure in Fuzhou basin and its vicinities by deep seismic reflection and high-resolution refraction as well as wide-angle reflection/refraction. Science in China Series D: Earth Sciences 48 (7), 925–938.

Zhu, J.S., Xuan, R.Q., Liu, K., Xu, H.B., Kon, Y.C., 2005. Study the structure of crust and upper mantle in east Asia and west Pacific marginal sea by Rayleigh surface wave. Computing Techniques for Geophysical and Geochemical Exploration 27 (3), 185–194.

Please cite this article as: Li, Q., et al., Seismic structure in the southeastern China using teleseismic receiver functions, Tectonophysics (2013), http://dx.doi.org/10.1016/j.tecto.2013.06.033